Journal of Alloys and Compounds 509 (2011) 3413–3418

Contents lists available at ScienceDirect

Journal of Alloys and Compounds

journal homepage: www.elsevier.com/locate/jallcom

Structure and upconversion luminescence properties of $BaYF_5$:Yb^{3+}, Er^{3+} nanoparticles prepared by different methods

Haiyan Du, Weihang Zhang, Jiayue Sun *

College of Chemistry and Environmental Engineering, Beijing Technology and Business University, Beijing 100048, China

ARTICLE INFO

Article history:
Received 26 May 2010
Received in revised form
12 December 2010
Accepted 15 December 2010
Available online 23 December 2010

Keywords:
Upconversion
Fluoride source
Co-precipitation technique
Hydrothermal synthesis

ABSTRACT

$BaYF_5$:Yb^{3+}, Er^{3+} (BYF) upconversion (UC) luminescence nanoparticles have been prepared using co-precipitation and hydrothermal techniques, respectively. Two different fluoride sources were used to synthesize BYF by the hydrothermal method, and the sizes of the as-prepared spherical particles were about 30 nm (NH_4BF_4 as a fluoride source) and 100 nm (NH_4HF_2 as a fluoride source), respectively. While the nanoparticles prepared by the co-precipitation method are irregular, many clusters and agglomerates can be seen. The UC fluorescence has been realized in all the as-prepared BYF samples upon 980 nm excitation. It is found that their luminescence spectra depend strongly upon the preparation method. Factors affecting the upconversion fluorescent intensity have been also studied. The UC emission transitions for $^4F_{9/2}$–$^4I_{15/2}$ (red), $^2H_{11/2}$–$^4I_{15/2}$ (green) and $^4S_{3/2}$–$^4I_{15/2}$ (green) in the Yb^{3+}/Er^{3+} codoped BYF nanoparticles depending on pumping power have also been discussed.

1. Introduction

Rare-earth (RE) doped nano-structured materials have attracted great interests in recent years due to luminescent properties induced by their nano-scale sizes with potential applications in the field of solid state luminescence [1–5]. Owing to high quantum efficiency and lower phonon energies, fluorides doped with RE ions are very attractive materials for optical applications, which are relatively stable in air and different from chloride or bromide hosts [6–8]. Among the RE ions, the Er^{3+} ion is suitable for converting infrared (IR) to the visible light through the upconversion (UC) process due to its proper electronic energy level scheme. The co-doping of the Yb^{3+} ion (a sensitizer) with the Er^{3+} ion can remarkably enhance the UC efficiency from infrared to visible lights due to the efficient energy transfer from Yb^{3+} to Er^{3+} [9–12].

Recently, many reports are focused on the modification of nano- to micro-sized fluoride phosphors, which involve selected solvent treatment, ligands and surfactants to control the size and morphology of the products. For example, Bu et al. synthesized novel Ba_2ErF_7 and Yb^{3+}-doped Ba_2ErF_7 powder by a co-precipitation method [13]. Chen et al. reported on the comparative investigation of structure and luminescence properties of tetragonal $LiYF_4$ and $BaYF_5$, and hexagonal $NaYF_4$ phosphors codoped with Er^{3+}/Yb^{3+} by a facile hydrothermal synthesis [14]. Furthermore, $BaYF_5$ in nanoscale is an ideal host for the Yb^{3+}/Tm^{3+} co-dopants [15], nevertheless a correlation between the synthesized phases and the luminescence behaviors is not clearly verified. Based on this, $BaYF_5$ can be used as a kind of ideal host for UC materials, and some researches on the shape- and size-dependent UC luminescent behavior of $BaYF_5$ are expected.

In the present work, the structure and upconversion luminescence properties of Yb^{3+}/Er^{3+} co-doped $BaYF_5$ samples prepared by different techniques have been studied. The particle sizes and the differences of upconversion spectra behavior between co-precipitation and hydrothermal techniques are described in detail.

2. Experimental

2.1. Synthesis

Yb^{3+}/Er^{3+}codoped $BaYF_5$ nanoparticles were prepared using co-precipitation and hydrothermal techniques, respectively, and the samples were named as c-BYF and h-BYF in the following section. All the BYF samples were co-doped with 20 mol% of Yb^{3+} and 6 mol% of Er^{3+} with respect to the alkali-earth metal ions. Analytical grade Er_2O_3, Yb_2O_3, and Y_2O_3 were separately dissolved in dilute HNO_3 to prepare the 0.2 mol/L stock solutions of $Er(NO_3)_3$, $Yb(NO_3)_3$, and $Y(NO_3)_3$. NH_4HF_2 and NH_4BF_4 were dissolved in deionized water to prepare the 1 mol/L stock solutions. For a typical synthesis of $BaYF_5$:20%Yb^{3+}/6%Er^{3+} nanocrystals, 0.5 mmol of stoichiometric $RE(NO_3)_3$ (0.2 mol/L, RE = Er, Yb, Y; Y:Yb:Er = 78:20:2) aqueous solution and 2 mL of fluoride solution (1 mol/L) were used.

2.1.1. Coprecipitation technique

For a typical co-precipitation synthesis procedure, 5 mmol (Ba^{2+}, 0.76Y^{3+}, 0.06Er^{3+}, and 0.2Yb^{3+}) was firstly mixed together, and then the mixture solution was added dropwise into25 mmol F^- (NH_4HF_2) ion solution under constant stirring. The obtained precipitate solutions were vigorously stirred at 50 °C for about 2 h. The white precipitate was separated by centrifugation and washed with water for several times, and then dried in a furnace at 100 °C for 24 h to obtain BYF precursors. The

* Corresponding author. Tel.: +86 010 6898 5467; fax: +86 010 6898 5467.
E-mail address: jiayue_sun@126.com (J. Sun).

0925-8388/$ – see front matter © 2010 Elsevier B.V. All rights reserved.
doi:10.1016/j.jallcom.2010.12.101

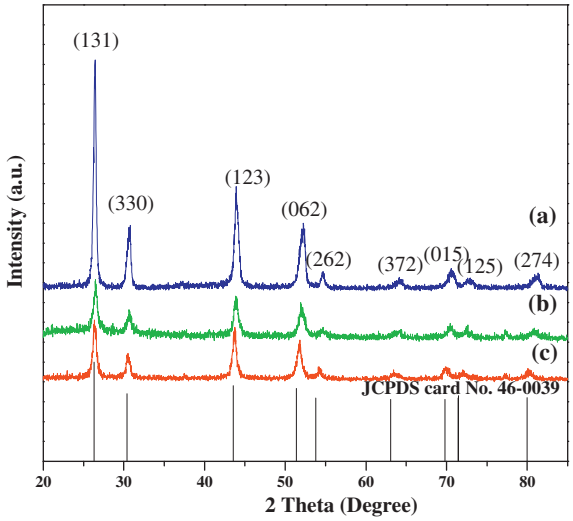

Fig. 1. XRD patterns of Yb^{3+}/Er^{3+} codoped BYF samples prepared by (a) co-precipitation technique, (b) hydrothermal technique by NH_4BF_4 source and (c) hydrothermal technique by NH_4HF_2 source. Bottom: JCPDS Powder Diffraction File Cards for $BaYF_5$.

precursors were subsequently annealed at 900 °C in air for 4 h to obtain the final product. The as-obtained sample was used for structure and property characterization.

2.1.2. Hydrothermal technique

For a typical hydrothermal synthesis procedure, 5 mmol (Ba^{2+}, 0.76Y^{3+}, 0.06Er^{3+}, and 0.2Yb^{3+}) was added in the 25 mL solution of the metal nitrates. Then 25 mmol F^- (NH_4HF_2/NH_4BF_4) ions should be necessary to precipitate totally metals as the fluoride by the reaction above transparent solution with vigorous stirring continuously for about 20 min. Subsequently, the milky colloidal solution was transferred to a 40 mL Teflon-lined autoclave, and the autoclave was sealed and maintained at 220 °C for 24 h, and then cooled to room temperature naturally. The white precipitate was separated by centrifugation and washed with ethanol for several times, and then dried in a vacuum at 80 °C for 12 h. The as-obtained sample was used for structure and property characterization.

2.2. Characterization

Powder X-ray diffraction (XRD) measurements were performed on a Shimadzu XRD-6000 diffractometer at a scanning rate of 2.0° (2θ)/min from 20° to 85°, with Cu Kα radiation (λ = 0.15405 nm). Transmission electron microscope (TEM) images were observed using a JEOL-2010 Electron Microscope with an acceleration voltage of 200 kV. Fourier transform infrared spectroscopy (FT-IR) data were collected on a Nicolet 380 spectrophotometer over the range of wavenumber 4000–1500 cm^{-1}. The photoluminescence (PL) measurements were performed on a HitachiF-4500 spectrophotometer equipped with a 150 W xenon lamp as the excitation source. The UC luminescence emission spectra were obtained on the same HitachiF-4500 spectrophotometer using a 980 nm semiconductor laser (Beijing Viasho Technology

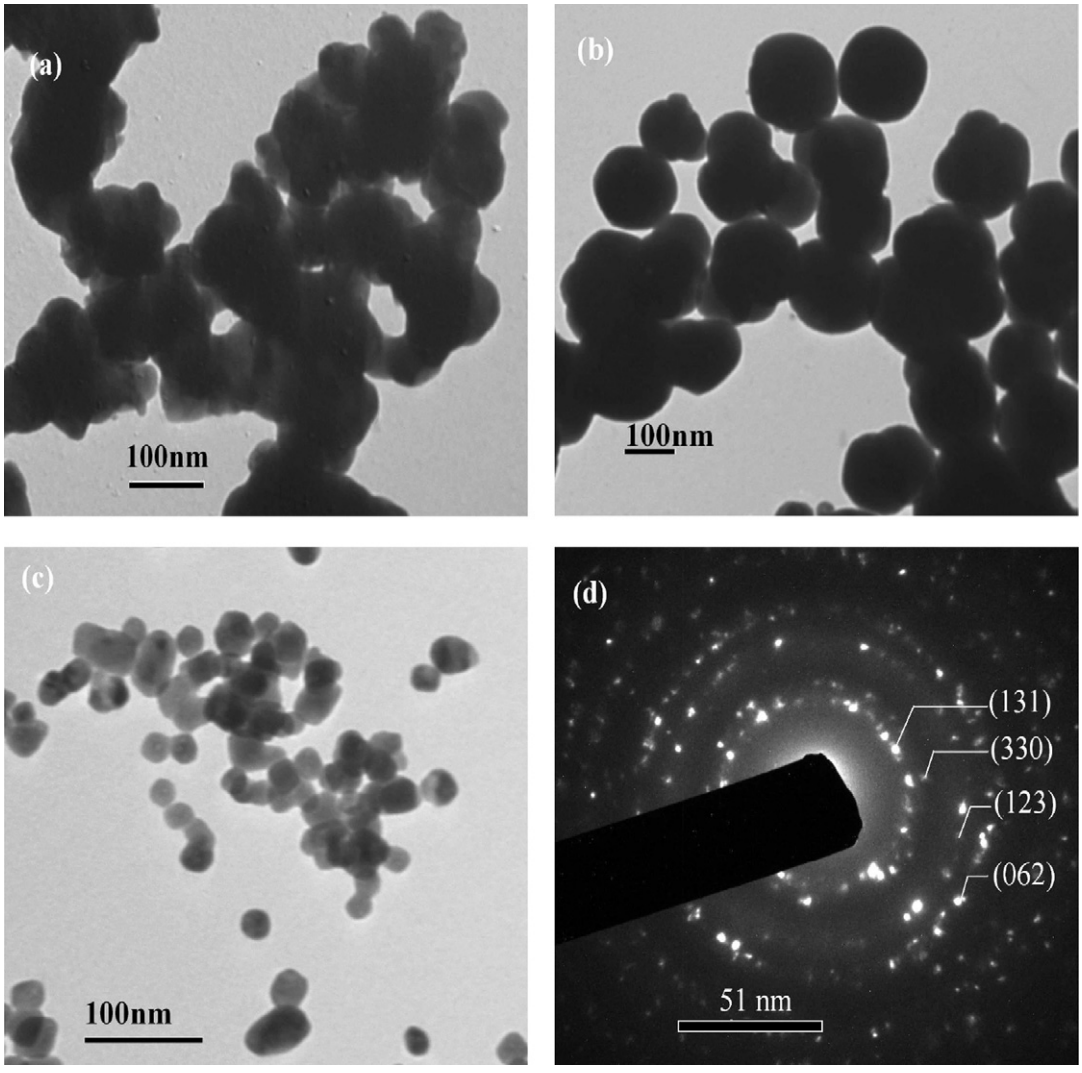

Fig. 2. TEM images of Yb^{3+}/Er^{3+} codoped BYF samples prepared by (a) co-precipitation, (b) hydrothermal by NH_4BF_4 source, (c) hydrothermal by NH_4HF_2 source techniques and (d) SAED pattern of h-BYF/NH_4HF_2.

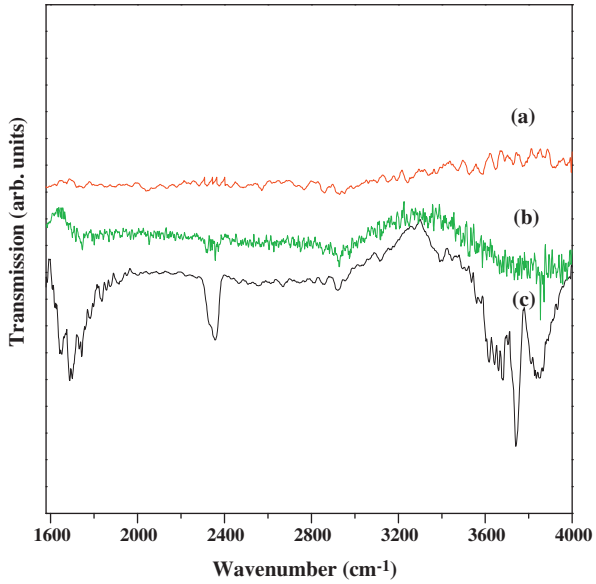

Fig. 3. IR reflectance spectra recorded for as-prepared c-BYF (a), h-BYF/NH_4BF_4 (b) and h-BYF/NH_4HF_2 (c).

Company, China) as the excitation source. All the measurements were performed at room temperature.

3. Results and discussion

3.1. XRD analysis

Fig. 1 gives the XRD patterns of the c-BYF samples (a), h-BYF samples using NH_4BF_4 as a fluoride source (h-BYF/NH_4BF_4) (b), and h-BYF samples using NH_4HF_2 as a fluoride source (h-BYF/NH_4HF_2) (c), respectively. All characteristic diffraction peaks at $2\theta = 26.3°$(1 3 1), 30.38°(3 3 0), 43.55°(1 2 3), 51.37°(0 6 2), 53.80°(2 6 2), 63.09°(3 7 2), 69.79°(0 1 5), 71.42°(1 2 5), and 79.98°(2 7 4) are presented, which are in good agreement with the standard values for the bulk tetragonal $BaYF_5$ (JCPDS46-0039). On the basis of the above results, we conclude that it cannot change the crystal structure of the products by varying different synthesis procedure and reaction condition. Further, it is found that the diffraction peaks all shift to the higher angles direction owing to the substitution of Er^{3+} and Yb^{3+} ions for Y^{3+}. As a result, the lattice parameters of $BaYF_5$:Yb^{3+}, Er^{3+} were calculated by the *Unit-Cell*program [16] in the tetragonal system based on the given XRD data in Fig. 1a, and it has an tetragonal phase and lattice constants of $a_C = 12.28 \pm 0.07$ Å, υ (cell volume) = 1010.99 ± 10.58 Å^3.

3.2. TEM analysis

TEM images were taken in order to estimate the size and evaluate the morphology of the grains of the BYF samples. A series of controlled experiments demonstrated that the shape evolutions of BYF crystals are influenced by external factors such as different methods and fluoride sources in conjunction with the intrinsic crystallographic structure of BYF crystals. Fig. 2 displays TEM images of the as-prepared c-BYF (a), h-BYF/NH_4BF_4 (b) and h-BYF/NH_4HF_2 (c). It is suggested that the crucial effects of synthesis conditions and fluoride sources on the crystalline phases and morphologies of the products in our current synthesis. As shown in Fig. 2a, it is found that the c-BYF grains consist of many clusters and agglomerates, which also has many particles with clearly marked grain boundaries. This result is characteristic of materials prepared at high sintering temperature. Differently from co-precipitation technique,

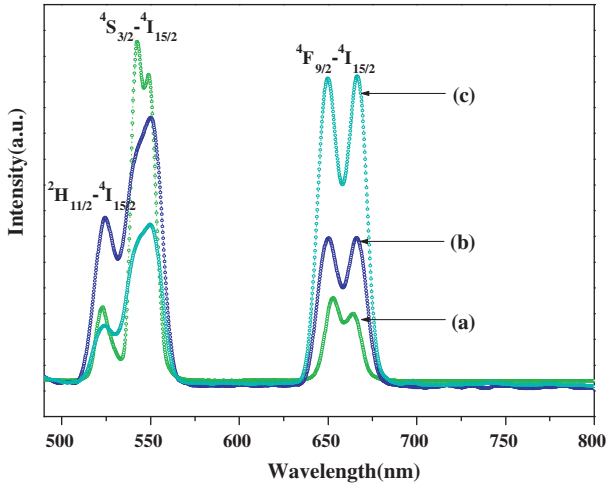

Fig. 4. Upconversion spectra of as-prepared c-BYF composites (a), h-BYF/NH_4BF_4 (b) and h-BYF/NH_4HF_2 samples (c).

the hydrothermal technique does not require high temperature treatments, avoiding agglomeration and sintering of the grains. Fig. 2b and c give the TEM images of the samples by hydrothermal method. For each h-BYF product, the grains do not form clusters and agglomerates as they are mostly separated and not sintered. When other reaction conditions remain invariable, the size of the obtained particles is about 100 nm if NH_4BF_4 is used as a fluoride source. However, NH_4HF_2 replaced NH_4BF_4 as the fluoride source, and the mean size of the obtained sample is about 30 nm in diameter (Fig. 2c). Meanwhile, the selected area electron diffraction (SAED) pattern for h-BYF/NH_4HF_2 sample (Fig. 2d) demonstrates the highly crystalline nature and confirmed the tetragonal crystalline structure of the h-BYF/NH_4HF_2 nanoparticles. By comparing the TEM images of the samples, the grain sizes of the BYF products formed under hydrothermal method are more uniform and small than that obtained by the co-precipitation method, meanwhile, the morphologies of the products are quite different from the different fluoride source in the same hydrothermal method.

For the hydrothermal method, in aqueous solution, BF_4^- (NH_4BF_4 as fluoride source) was hydrolyzed to produce BO_3^{3-}, HF and F^- anions, as shown in the following Eq. (1), and then F^- anions

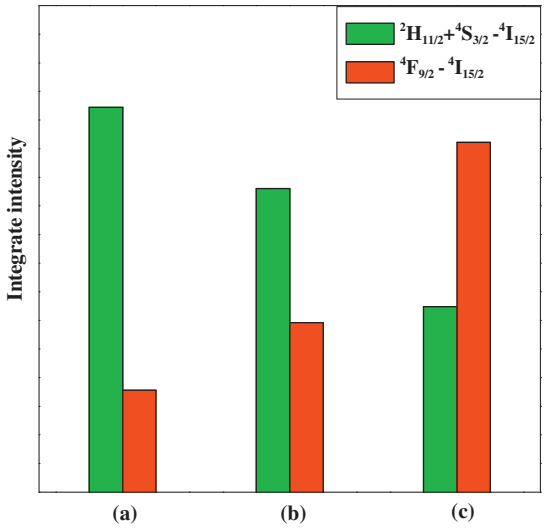

Fig. 5. Different integrated green ($^2H_{11/2} + {}^4S_{3/2} - {}^4I_{15/2}$) to red ($^4F_{9/2} - {}^4I_{15/2}$) upconversion emission intensity of as-prepared c-BYF composites (a), h-BYF/NH_4BF_4 (b) and h-BYF/NH_4HF_2 samples (c).

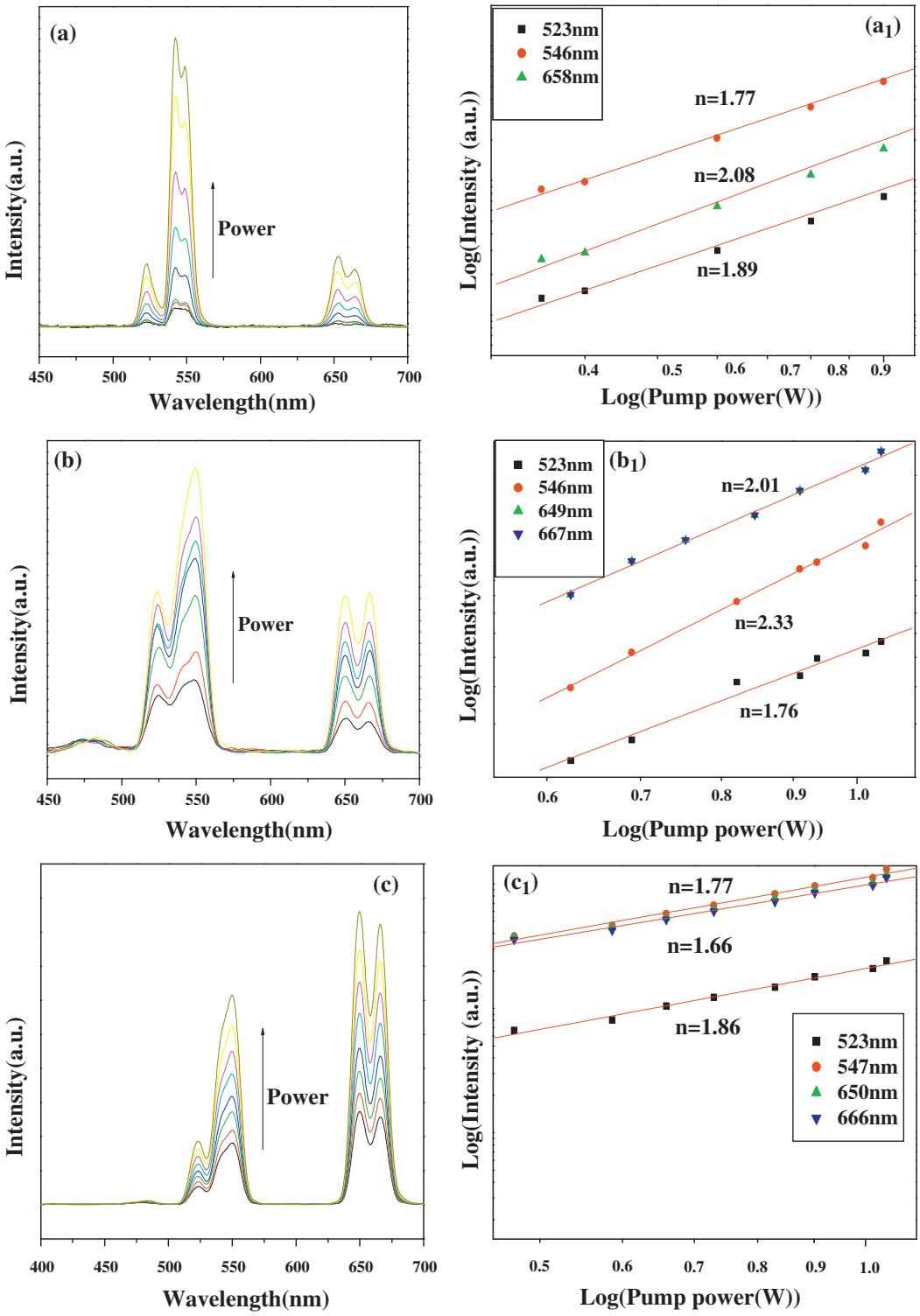

Fig. 6. Power dependent upconversion spectra of c-BYF (a), h-BYF/NH_4BF_4 (b) and h-BYF/NH_4HF_2 samples, and the right shows log–log plots of $^2H_{11/2}(^4S_{3/2})$–$^4I_{15/2}$ (green), and $^4F_{9/2}$–$^4I_{15/2}$ (red) transition emissions of c-BYF (a_1), h-BYF/NH_4BF_4 (b_1) and h-BYF/NH_4HF_2 (c_1) samples versus pump power, respectively. (For interpretation of the references to color in this figure legend, the reader is referred to the web version of this article.)

react with Ba^{2+}, Y^{3+} to form BYF shown in Eq. (3). As a comparison, HF_2^- (NH_4HF_2 as fluoride source) was directly hydrolyzed to produce HF and F^- anions, as shown in the following Eq. (2), and then F^- anions react with Ba^{2+}, Y^{3+} to form BYF shown in Eq. (3). It is found that the equilibrium constant of the hydrolysis reaction [Eqs. (1) and (2)] is different in the present hydrothermal condition, which will induce different morphologies and sizes of the nanoparticles [17].

$$BF_4^- + 3H_2O \leftrightarrow H_3BO_3 + 3HF + F^- \quad (1)$$

$$HF_2^- \leftrightarrow HF + F^- \quad (2)$$

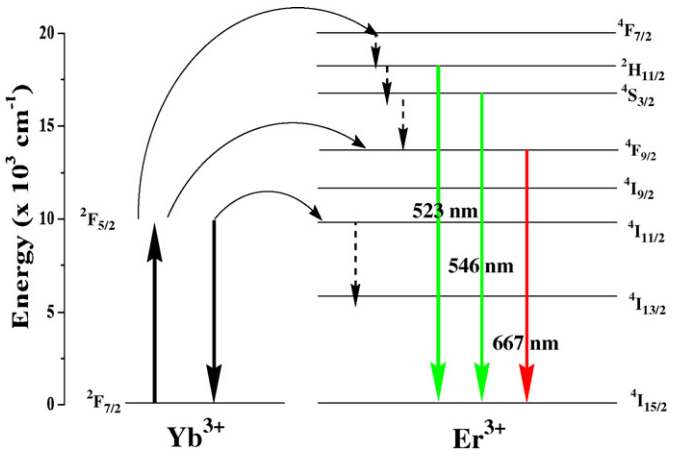

Fig. 7. Schematic energy levels of Yb^{3+} and Er^{3+} ions in the as-prepared $BaYF_5$:Yb^{3+}, Er^{3+} samples.

$$Ba^{2+} + Y^{3+} + 5F^- \rightarrow \text{BYF} \downarrow \quad (3)$$

3.3. IR spectra and optical characterization

Fig. 3 presents IR reflectance spectra recorded for as-prepared c-BYF (a), h-BYF/NH_4BF_4 (b) and h-BYF/NH_4HF_2 (c). As expected, the as-prepared h-BYF samples contain considerable amounts of water. Meanwhile, the content of water in h-BYF/NH_4HF_2 (c) is larger than for as-prepared h-BYF/NH_4BF_4 sample. These are evidenced by the broad band around 3740 cm^{-1} as well as narrower band observed at 1640 cm^{-1}, indicative of antisymmetric and symmetric stretches and HOH bending modes [18]. Fig. 4 shows the UC emission spectra of as-prepared c-BYF (a), h-BYF/NH_4BF_4 (b) and h-BYF/NH_4HF_2 (c) upon an excitation wavelength of 980 nm, all of which have similar spectra profile corresponding to the same wavelength except for different relative emission intensities. Three intense emission bands centered at 523, 546, and 667 nm corresponding to the transitions of $^4S_{3/2}$–$^4I_{15/2}$, $^2H_{11/2}$–$^4I_{15/2}$ and $^4F_{9/2}$–$^4I_{15/2}$, respectively, were simultaneously observed. It can be seen that the upconversion fluorescence intensities of green (523 and 546 nm) and red {667 nm} emissions of Er^{3+} are affected by the different methods. The UC intensity of green emission for c-BYF is larger than that of as-prepared h-BYF samples. However, the strongest emission peak occurs at 667 nm in h-BYF/NH_4HF_2 samples (Fig. 4c). Fig. 5 shows the different integrated ratios for the green ($^2H_{11/2} + {}^4S_{3/2} - {}^4I_{15/2}$) and red ($^4F_{9/2} - {}^4I_{15/2}$) upconversion emission based on the different samples. Since the component and crystal structure are the same for c-BYF and h-BYF samples, heat-treatment temperature then becomes the reason for why they have different upconversion spectra. The very large difference in the heat-treatment temperature may have an effect on the amount of the impurity which then affects the luminescence behaviors [19]. The c-BYF samples were heat-treated at 900 °C finally, while the h-BYF samples were heated only at 80 °C. So sample heated at 80 °C will have considerable amount of the water and hydroxyl groups, probably that bounded to the surface of the powder evaporates; however, heating at 900 °C is necessary for complete removing of the stronger bounded hydroxyl groups [20,21]. Thus, the energy in the $^4S_{3/2}$ level for the green emission will be relaxed to the lower $^4F_{9/2}$ level, increasing the red-to-green ratio of the emission. This results from a considerable amount of water and hydroxyl groups present in the fluoride structure, which quenches the emission from the higher positioned levels [22–24]. Therefore, the water and hydroxyl groups can explain why the differences in emission spectra exist between c-BYF and h-BYF.

Further, Fig. 6 gives the pumping power dependent upconversion spectra of BYF samples, suggesting that UC emission intensities increased gradually with increasing pumping power. Different UC emission intensities are observed for the three BYF samples. To investigate the fundamental UC mechanism of samples, the right presents the pumping power dependence of $^2H_{11/2}$($^4S_{3/2}$)–$^4I_{15/2}$ (green) and $^4F_{9/2}$–$^4I_{15/2}$ (red) transition emissions for as-prepared BYF samples. It is well known that the emission intensity (I_f) will be proportional to some power (n) of the infrared excitation power (P) [25]:

$$I_f \propto P^n \quad (4)$$

where $n$is the number of photons required to populate the emitting state. The results are shown in Fig. 6 for different samples. These results show that two-photon process is responsible for green and red emissions to the three BYF samples. The excited states for upconversion can be populated by several well-known mechanisms: (1) excited state absorption (ESA) and (2) energy transfer (ET) [26–28]. Fig. 7 shows the energy level diagram of Er^{3+} and Yb^{3+} ions as well as the proposed upconversion mechanisms accounting for the green and red emissions under 980 nm laser excitation [29–31]. In the complex Yb^{3+}/Er^{3+}codoped BYF system, an initial energy transfer from an Yb^{3+} ion in the $^2F_{5/2}$ state to an Er^{3+} ion populates the $^4I_{11/2}$ level. A second 980 nm photon, or energy transfer from an Yb^{3+} ion, can then populate the $^4F_{7/2}$ level of the Er^{3+} ion. The Er^{3+} ion can then relax nonradiatively to the $^2H_{11/2}$ and $^4S_{3/2}$ levels, and the green $^2H_{11/2}$–$^4I_{15/2}$ and $^4S_{3/2}$–$^4I_{15/2}$ emissions occur. Alternatively, the ion can further relax and populate the $^4F_{9/2}$ level leading to the red $^4F_{9/2}$–$^4I_{15/2}$ emission. The $^4F_{9/2}$ level may also be populated from the $^4I_{13/2}$ level of the Er^{3+} ion by absorption of a 980 nm photon, or energy transfer from an Yb^{3+} ion, with the $^4I_{13/2}$ state being initially populated via the nonradiative$^4I_{11/2}$–$^4I_{13/2}$ relaxation [21].

4. Conclusions

$BaYF_5$:Yb^{3+}, Er^{3+} (BYF) materials have been prepared using two different techniques. The size and morphology of the as-prepared particles depend upon the preparation technique. The UC fluorescence has been realized in the as-prepared BYF samples upon 980 nm excitation. The UC emission transitions for both $^2H_{11/2}$ ($^4S_{3/2}$)–$^4I_{15/2}$ (green) and $^4F_{9/2}$–$^4I_{15/2}$ (red) in the BYF:Yb^{3+}, Er^{3+} samples came from two-photon UC processes. Obvious differences in fluorescent emission spectra between c-BYF and h-BYF powders were observed. The UC intensity of green emission in c-BYF is larger than that of as-prepared h-BYF samples, while the strongest emission peak occurs at 667 nm in h-BYF/NH_4HF_2 samples. The impurities of water and hydroxyl groups and the surface effect were suggested to account for the upconversion luminescence differences between the c-BYF and the h-BYF materials.

Acknowledgements

This work was supported by the National Natural Science Foundation of China (No. 20976002 and No. 20876002), the Beijing Natural Science Foundation (No. 2091002, and No. 2082009), and Funding Project for Academic Human Resources Development in the Institution of Higher Learning Under the Jurisdiction of Beijing Municipality.

References

[1] F.Z. Shan, D.Q. Chen, Y.L. Yu, P. Huang, F.Y. Weng, H. Lin, Y.H. Wang, Mater. Res. Bull. 45 (2010) 1017–1020.
[2] L. Kassab, F. Bomfim, J. Martinelli, N. Wetter, J. Neto, C.B. de Araujo, Appl. Phys. B 94 (2009) 239–242.

[3] Z.G. Chen, Q.W. Tian, Y.L. Song, J.M. Yang, J.Q. Hua, J. Alloys Compd. 506 (2010) L17–L21.
[4] W.P.Q.D.S. Zhang, D. Zhao, L.L. Wang, K.Z. Zheng, Chem. Commun. 46 (2010) 2304–2306.
[5] Y.Q. Qu, X.G. Kong, Y.J. Sun, Q.H. Zeng, H. Zhang, J. Alloys Compd. 485 (2009) 493–496.
[6] F.Y. Weng, D.Q. Chen, Y.S. Wang, Y.L. Yu, P. Huang, H. Lin, Ceram. Int. 35 (2009) 2619–2623.
[7] G.J. De, W.P. Qin, J.S. Zhang, J.S. Zhang, Y. Wang, C.Y. Cao, Y. Cui, J. Lumin. 122–123 (2007) 128–130.
[8] G.F.W. Wang, P. Qin, J.S. Zhang, L.L. Wang, G.D. Wei, P.F. Zhu, R. Kim, J. Alloys Compd. 475 (2009) 452–455.
[9] F. Wang, Y. Han, C.S. Lim, Y. Lu, J. Wang, J. Xu, H. Chen, C. Zhang, M. Hong, X. Liu, Nature 463 (2010) 1061.
[10] E.Y. Lee, M. Nazarov, Y.J. Kim, J. Electrochem. Soc. 157 (2010) J102–J107.
[11] R. Kapoor, C.S. Friend, A. Biswas, P.N. Prasad, Opt. Lett. 25 (2000) 338–340.
[12] F. Vetrone, J.C. Boyer, J.A. Capobianco, J. Phys. Chem. B 107 (2003) 1107–1112.
[13] Y.Y. Bu, S.G. Xiao, X.F. Wang, W.H. Yuan, J.W. Ding, J. Lumin. 130 (2010) 38–44.
[14] X.P. Chen, Q.Y. Zhang, C.H. Yang, D.D. Chen, C. Zhao, Spectrochim. Acta A 74 (2009) 441–445.
[15] F. Vetrone, V. Mahalingam, J.A. Capobianco, Chem. Mater. 21 (2009) 1847–1856.
[16] T.J.B. Hollandm, S.A.T. Redfern, Mineral. Mag. 61 (1997) 65–69.
[17] C.X. Li, J. Yang, P.P. Yang, H.Z. Lian, J. Lin, Chem. Mater. 20 (2008) 4317–4326.
[18] K. Nakamoto, Infrared and Raman Spectra of Inorganic and Coordination Compounds, Wiley, New York, 1978, p. 227.
[19] N. Martin, P. Boutinaud, R. Mahiou, J.-C. Cousseins, M. Bouderbala, J. Mater. Chem. 9 (1999) 125–128.
[20] A. Mech, M. Karbowiak, L. Kepiniński, A. Bednarkiewicz, W. Strek, J. Alloys Compd. 380 (2004) 315–318.
[21] M. Karbowiak, A. Mech, A. Bednarkiewicz, W. Strek, L. Kepinski, J. Phys. Chem. Solids 66 (2005) 1008–1019.
[22] J.-C. Boyer, L.A. Cuccia, J.A. Capobianco, Nano Lett. 7 (2007) 847–852.
[23] M.Y. Xie, X.N. Peng, X.F. Fu, J.J. Zhang, G.L. Lia, X.F. Yu, Scripta Mater. 60 (2009) 190–193.
[24] C.M. Zhang, Z.Y. Hou, R.T. Chai, Z.Y. Cheng, Z.H. Xu, C.X. Li, L. Huang, J. Lin, J. Phys. Chem. C 114 (2010) 6928–6936.
[25] Q.L. Dai, H.W. Song, X.G. Ren, S.Z. Lu, G.H. Pan, X. Bai, B. Dong, R.F. Qin, X.S. Qu, H. Zhang, J. Phys. Chem. C 112 (2008) 19694–19698.
[26] H. Guo, Y.M. Qiao, Opt. Mater. 31 (2009) 583–589.
[27] F. Vetrone, J.C. Boyer, J.A. Capobianco, A. Speghini, M. Bettinelli, Chem. Mater. 15 (2003) 2737–2743.
[28] J.A. Capobianco, F. Vetrone, J.C. Boyer, A. Speghini, M. Bettinelli, J. Phys. Chem. B 106 (2002) 1181–1187.
[29] H. Guo, N. Dong, M. Yin, W.P. Zhang, L.R. Lou, S.D. Xia, J. Phys. Chem. B 108 (2004) 19205–19209.
[30] H. Guo, Opt. Mater. 29 (2007) 1840–1843.
[31] H. Lin, G. Meredith, S. Jiang, X. Peng, T. Luo, N. Peyghambarian, E.Y. Pun, J. Appl. Phys. 93 (2003) 186–191.